Cancer Letters 385 (2017) 12–20

Contents lists available at ScienceDirect

Cancer Letters

journal homepage: www.elsevier.com/locate/canlet

Original Article

Dying glioma cells establish a proangiogenic microenvironment through a caspase 3 dependent mechanism

Xiao Feng [a, 1], Yang Yu [a, 1], Sijia He [a], Jin Cheng [a], Yanping Gong [a], Zhengxiang Zhang [a], Xuguang Yang [a], Bing Xu [a], Xinjian Liu [a], Chuan-Yuan Li [b, ***], Ling Tian [c, **], Qian Huang [a, *]

[a] The Comprehensive Cancer Center and Shanghai Key Laboratory for Pancreatic Diseases, Shanghai General Hospital, Shanghai Jiao Tong University School of Medicine, Shanghai 201620, China
[b] The Department of Dermatology, Duke University Medical Center, Durham, NC 27710, USA
[c] Institute of Translational Medicine and Shanghai Key Laboratory for Pancreatic Diseases, Shanghai General Hospital, Shanghai Jiao Tong University School of Medicine, Shanghai 201620, China

ARTICLE INFO

Article history:
Received 19 July 2016
Received in revised form
19 October 2016
Accepted 22 October 2016

Keywords:
Irradiation
Caspase 3
Angiogenesis
COX-2/PGE_2
VEGF-A

ABSTRACT

Vascular recovery or re-angiogenesis after radiotherapy plays a significant role in tumor recurrence, whereas molecular mechanisms of this process remain elusive. In this work, we found that dying glioma cells promoted post-irradiation angiogenesis through a caspase 3 dependent mechanism. Evidence *in vitro* and *in vivo* indicated that caspase 3 inhibition undermined proangiogenic effects of dying glioma cells. Proteolytic inactivation of caspase 3 in glioma cells reduced tumorigenicity. Importantly, we identified that NF-κB/COX-2/PGE_2 axis acted as downstream signaling of caspase 3, mediating proangiogenic response after irradiation. Additionally, VEGF-A, regulated by caspase 3 possibly through phosphorylated eIF4E, was recognized as another downstream factor participating in the proangiogenic response. In conclusion, these data demonstrated that caspase 3 in dying glioma cells supported the proangiogenic response after irradiation by governing NF-κB/COX-2/PGE_2 axis and p-eIF4E/VEGF-A signaling. While inducing caspase 3 activation has been a generally-adopted notion in cancer therapeutics, our study counterintuitively illustrated that caspase 3 activation in dying glioma cells unfavorably supported post-irradiation angiogenesis. This double-edged role of caspase 3 suggested that taming caspase 3 from the opposite side, not always activating it, may provide novel therapeutic strategies due to restricted post-irradiation angiogenesis.

Introduction

Gliomas, accounting for almost 80% of primary malignant brain tumors [1], are a devastating disease with uncontrollable proliferation and invasion, damage to surrounding brain tissue and profound neurological dysfunction [2,3]. In spite of endeavors to exploit new therapeutic strategies for gliomas [4–7], gliomas cunningly develop different compensatory mechanisms [8–11], leading to therapy resistance and unfavorable prognosis. For example, astrocytomas, including glioblastomas (GBMs), can establish microtube-dependent cell interconnection and form functional multicellular network, which protect tumor cells from radiotherapy-induced cell death and develop radioresistance [12].

Though radioresistance widely exists in gliomas, radiotherapy has long been the primary therapeutic modality for unresectable gliomas and also acts as the standard adjuvant approach in glioma treatment [13]. Nonetheless, in almost all patients with malignant gliomas, recurrence following initial treatment, including radiotherapy, inevitably occurs and represents grim outcomes [14]. Glioma growth and progression is heavily reliable on angiogenesis [15]. Thus, it is conceivable that vascular recovery or re-angiogenesis plays a crucial role in glioma recurrence following radiotherapy. For instance, evidence from both mice [16] and human specimens [17] suggested that the angiogenic pattern of

Abbreviations: COX-2, cyclooxygenase-2; PGE_2, prostaglandin E_2; eIF4E, eukaryotic initiation factor 4E; VEGF-A, vascular endothelial growth factor-A; GBM, glioblastoma.

* Corresponding author. Fax: +86 21 63240825.
** Corresponding author. Fax: +86 21 63240825.
*** Corresponding author. Fax: +86 21 63240825.
E-mail addresses: chuan.li@duke.edu (C.-Y. Li), tl09168@hotmail.com (L. Tian), qhuang@sjtu.edu.cn (Q. Huang).

[1] These authors contributed equally to this work.

http://dx.doi.org/10.1016/j.canlet.2016.10.042
0304-3835/

CXCL12-CXCR4 pathway may be responsible for GBM recurrence after radiotherapy.

Therefore, unveiling the proangiogenic mechanisms of glioma after radiotherapy is of great importance, because it would aid us in developing more useful strategies to reduce glioma recurrence following radiotherapy. One group reported that ionizing irradiation-induced MMP-9 upregulation promoted medulloblastoma angiogenesis by enhancing syndecan-1 shedding [18]. Another study demonstrated that depletion of DNA-dependent protein kinase catalytic subunit in GBM cells partly diminished irradiation induced-angiogenesis, with decreased VEGF secretion [19].

While these studies discovered important mechanisms underlying post-irradiation angiogenesis in gliomas, we still hope to identify the initial proangiogenic factor buried in the irradiated glioma microenvironment. Because ionizing irradiation induces a vast amount of glioma cell death, we hypothesize that these dying glioma cells may act as supporters, inflicting strong proangiogenic impacts on surrounding microenvironment.

Caspase 3 has been well established to function as executioner during cell apoptosis. However, accumulating interesting studies have identified growth-promoting roles of caspase 3 under various circumstances, such as fibrosis [20], wound healing and tissue regeneration [21], tumor repopulation [22], osteoclastogenesis [23] and oncogenic transformation [24]. Here, we therefore investigated whether caspase 3 in dying glioma cell mediated the proangiogenic effects following irradiation. We hope this caspase 3-mediated proangiogenic pathway could provide new therapeutic strategies to reduce glioma recurrence after radiotherapy.

Materials and methods

Cell culture and irradiation

U-87 MG (U87), human umbilical vein endothelial cells (HUVECs) and human dermal microvascular endothelial cells (HMEC-1) were cultured in Dulbecco's Modified Eagle's Medium (DMEM) (Thermo Fisher Scientific, MA, USA) with supplementation of 10% fetal bovine serum (FBS) (Gibco, life technologies, Auckland, NZ). X-ray irradiation for cells was performed with an ONCOR linear accelerator (Siemens, Amberg, Germany), whose dose rate is 3.6 Gy/min.

Gene transduction

The pLEX lentiviral vector system (Open Biosystem, Huntsville, AL, USA) was used to transduce exogenous genes into target cells. The firefly luciferase (Fluc) and green fluorescent protein (GFP) fusion gene [22] and dominant-negative caspase 3 [22,24] with a key cysteine mutation in the catalytic domain of caspase 3 (C163A) were provided by Prof. Chuan-Yuan Li. Lentiviral vectors were packaged into live, replication-deficient lentivirus in 293T cells following the manufacturer's instructions. HUVEC-Fluc, HMEC-1-Fluc and U87 CASP3DN were constructed through lentivirus infection and subsequent puromycin selection at 3 μg/ml.

Measurement of endothelial cell proliferation with bioluminescence imaging

We used bioluminescence imaging to measure endothelial cell proliferation, because luciferase activity of Fluc-labeled endothelial cells was validated to be tightly correlated cell numbers. HUVEC-Fluc or HMEC-1-Fluc (100 cells) were seeded onto (1.5×10^4) of differentially irradiated U87 cells within 24 h after irradiation in 24-well plates. For transwell assay, HUVEC-Fluc were seeded onto hanging cell culture inserts of 0.4 μm pore size (PIHT12R48; Millipore, MA, USA). During the coculture period (7–10 days), culture medium was replaced by fresh 2% FBS DMEM every 2 days. Finally, to measure luciferase activity of HUVEC-Fluc and HMEC-1-Fluc, D-Luciferin potassium (bc219; Synchem UG & Co. KG, Felsberg/Altenburg, Germany) diluted in PBS (0.15 mg/ml) was added into each well before bioluminescence imaging.

Machines for bioluminescence imaging used in this study were NC100 instrument (Berthold Technologies GmbH & Co. KG, Bad Wildbad, Germany), SPECTRAL Ami X (Spectral Instruments Imaging, Tucson, AZ, USA) and IVIS Lumina Series III (PerkinElmer, USA).

Conditioned medium preparation

Equal numbers of tumor cells were seeded into cell culture dishes overnight. Culture medium was replaced by low serum medium (2% FBS) before irradiation. 48 h after irradiation, culture medium was collected, centrifuged at 3000 rpm for 10 min, filtered with 0.22 μm filter unit and stored at −80 °C until use.

HUVEC migration assay

HUVEC migration was conducted with hanging cell culture inserts of 8 μm pore size (PIEP12R48; Millipore) for 24-well plates. Briefly, 600 μl conditioned medium was added into the lower chamber of every well and 200 μl serum free DMEM containing HUVECs (3×10^4) added on the top of inserts. 16–18 h later, HUVECs staying in the inserts were gently removed with cotton swabs. Migratory HUVECs were fixed with 4% paraformaldehyde and stained with crystal violet. Number of migratory HUVECs was measured by counting cells from five random fields under microscope.

Flow cytometric analysis

Cell apoptosis was detected by Accuri C6 Flow cytometer (BD Biosciences, CA, USA) with FITC Annexin V apoptosis detection kit (556547; BD Pharmingen™, San Diego, CA, USA). Procedures were conducted in accordance with the technical data sheet from the kit.

Confocal microscopy for phosphorylated histone H2A.X and cleaved caspase 3

Confocal microscopy was mainly performed as described [20]. Primary antibodies used here were phosphorylated histone H2A.X and cleaved caspase 3 (#9718; #9664; Cell Signaling Technology, MA, USA).

Western blot

Western blot analysis was performed as previously described [25]. Primary antibodies were against HA-tag, β-actin, COX-2, phospho-p65, caspase 3, cleaved caspase 3 and phospho-eIF4E (#3724; #4967; #12282; #3033; #9662; #9664; #9741; Cell Signaling Technology).

Matrigel plug assay

To perform matrigel plug assay, we used female nude mice at 4–6 weeks old. For each mice, 500 μl matrigel mixed with 2×10^6 either U87 or U87 CASP3DN cells treated with 10 Gy irradiation was subcutaneously implanted into either flank of three mice, respectively. 12 days after implantation, three mice were sacrificed and six plugs (three plugs containing irradiated U87 cells and the other three containing irradiated U87 CASP3DN cells) were collected. Skin vasculature formation adjacent to plugs was photographed (the number of independent plug-adjoining vasculature is three because there are three plug replicates) and then length of vessels and diameter of major vessels were evaluated with the software ImageJ.

Immunohistochemistry analysis

Immunohistochemistry analysis was conducted as previously described [26]. Primary antibody used here was against CD34 (#3569; Cell Signaling Technology) and VWF (sc-14014; Santa Cruz Biotechnology). The number of analyzed plug sections for immunohistochemistry analysis is five. The area of vessels was quantified with the software ImageJ.

Tumor xenograft assay

Female nude mice at 4–6 weeks old were utilized for tumor xenograft experiment. 100 μl PBS containing 2.5×10^6 U87 or U87 CASP3DN was subcutaneously injected into either hind leg, respectively. Every week tumor size was measured and tumor volume (V) was calculated according to the formula: $V = 0.5 \times \text{length} \times \text{width}^2$.

In silico analysis of correlation between CASP3 and angiogenesis markers

The 169 RNA-seq data from 161 GBM cases were acquired from TCGA (The Cancer Genome Atlas, http://cancergenome.nih.gov/). The original count data of RNA-seq were normalized with edgeR package [27] in R.

We also downloaded the microarray data from 220 glioma patients from CGGA (the Chinese Glioma Genome Atlas, http://www.cgga.org.cn/index.php?m=Page&a=index&id=42).

Enzyme-linked immunosorbent assay (ELISA)

To measure the PGE_2 concentration of cell culture supernatants, we used Prostaglandin E_2 Express ELISA Kit (500141; Cayman Chemical, MI, USA). To detect the VEGF-A concentration of supernatants, we used Human VEGF Valukine ELISA Kit (VAL106; R&D Systems, MN, USA). Procedures were carried out according to the guidebooks in the kits.

Other drugs

NS-398 and Z-DEVD-FMK were bought from Cayman Chemical and Ki8751 was from Selleckchem (TX, USA).

Ethics

All animal procedures were performed in accordance with the Animals (scientific procedures) Act 1986 and also approved by the Animal Care Committee at Shanghai General Hospital.

Statistical analysis

Statistical analysis was conducted using SPSS 20.0 (IBM, USA). All data were presented as mean ± SEM (standard error of the mean). In parametric tests, unpaired Student's *t*-test was used for two-group test and one-way analysis of variance (one-way ANOVA) was used for multi-group test. The post-hoc analysis after ANOVA we employed was least significant difference (LSD). In non-parametric tests, Mann–Whitney *U* test was used to compare two groups of data that do not follow normal distributions. Spearman correlation analysis was taken to examine the correlation between CASP3 and angiogenesis markers. Difference was regarded statistically significant when p value was less than 0.05.

Results

Irradiated glioma cells activate endothelial cells in vitro

We firstly compared the radio-sensitivity of two model cells (U87 cells and HUVECs) in this work (Fig. S1). To investigate the proangiogenic property of irradiated glioma cells, we examined how irradiated glioma cells affect endothelial proliferation and migration, which are two essential processes for angiogenesis. To determine whether irradiated glioma cells promote endothelial proliferation, we took advantage of the following *in vitro* coculture model. Briefly, a small number (100 cells) of HUVEC-Fluc or HMEC-1-Fluc, were seeded onto a larger number (1.5×10^4) of differentially irradiated U87 cells, described as feeder cells. Following a 7–10 day coculture

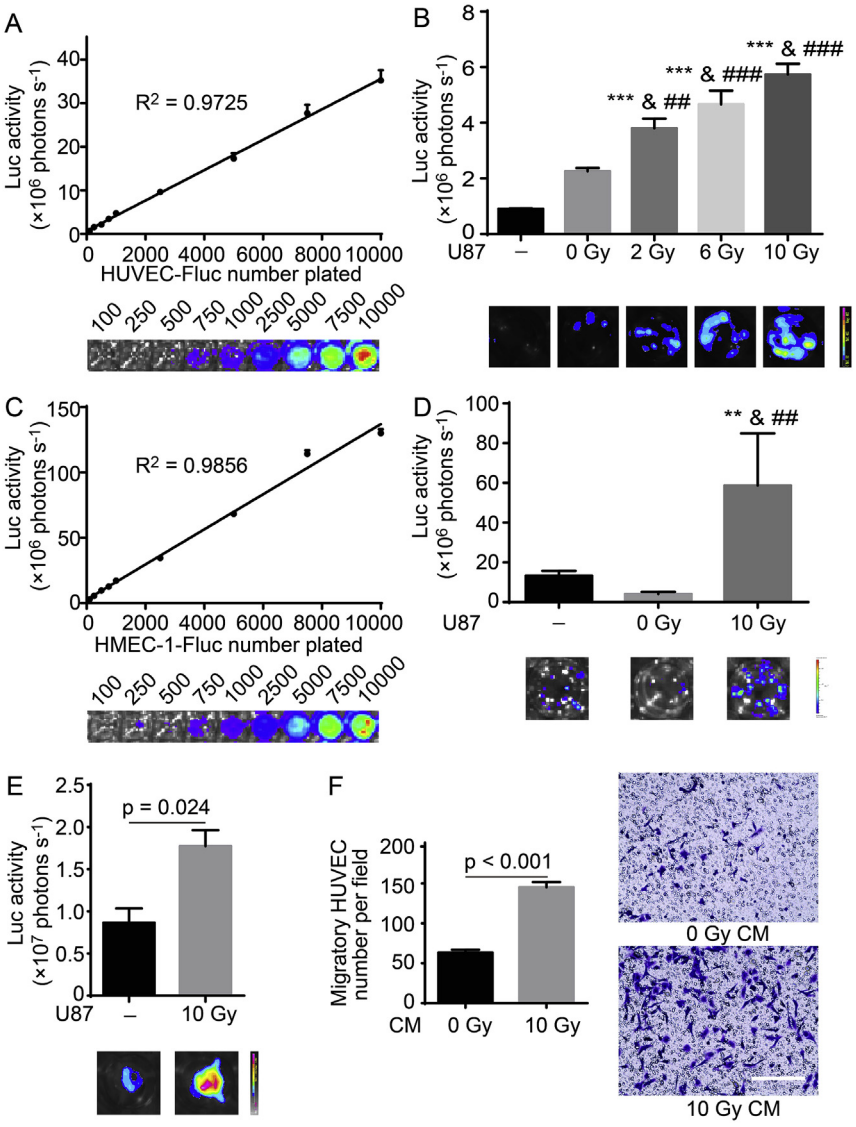

Fig. 1. Irradiated U87 cells activate endothelial cells. **A**. Linear correlation ($R^2 = 0.9725$) between luciferase activity of HUVEC-Fluc and cell number plated. **B**. Irradiated U87 cells stimulated HUVEC-Fluc proliferation. Upper panel, growth of HUVEC-Fluc alone or cocultured with variously irradiated or non-irradiated U87 cells was evaluated by bioluminescence imaging. ***p < 0.001, compared with HUVEC-Fluc alone, one-way ANOVA, LSD, n = 4. ##p < 0.01, ###p < 0.001, compared with non-irradiated, one-way ANOVA, LSD, n = 4. Lower panel, representative bioluminescence images. **C**. Linear correlation ($R^2 = 0.9856$) between luciferase activity of HMEC-1-Fluc and cell number plated. **D**. 10 Gy-irradiated U87 cells promoted HMEC-1-Fluc proliferation. Upper panel, proliferation of HMEC-1-Fluc cocultured with differently treated U87 cells was tested by bioluminescence imaging. **p < 0.01, compared with HMEC-1-Fluc alone, one-way ANOVA, LSD, n = 4. ##p < 0.01, compared with non-irradiated, one-way ANOVA, LSD, n = 4. Lower panel, representative bioluminescence images. **E**. Proliferation-promoting effect of 10 Gy-irradiated U87 cells on HUVEC-Fluc plated in hanging inserts. Upper panel, proliferation of HUVEC-Fluc cocultured with 10 Gy-irradiated U87 cells or not was measured by bioluminescence imaging (p = 0.024, Student's *t*-test, n = 3). Lower panel, representative bioluminescence images. **F**. Left panel, quantification analysis showing HUVEC migration towards different conditioned media (CM) (p < 0.001, Student's *t*-test, n = 5). Right panel, representative images of HUVEC migration towards indicated CM. Scale bar: 250 μm.

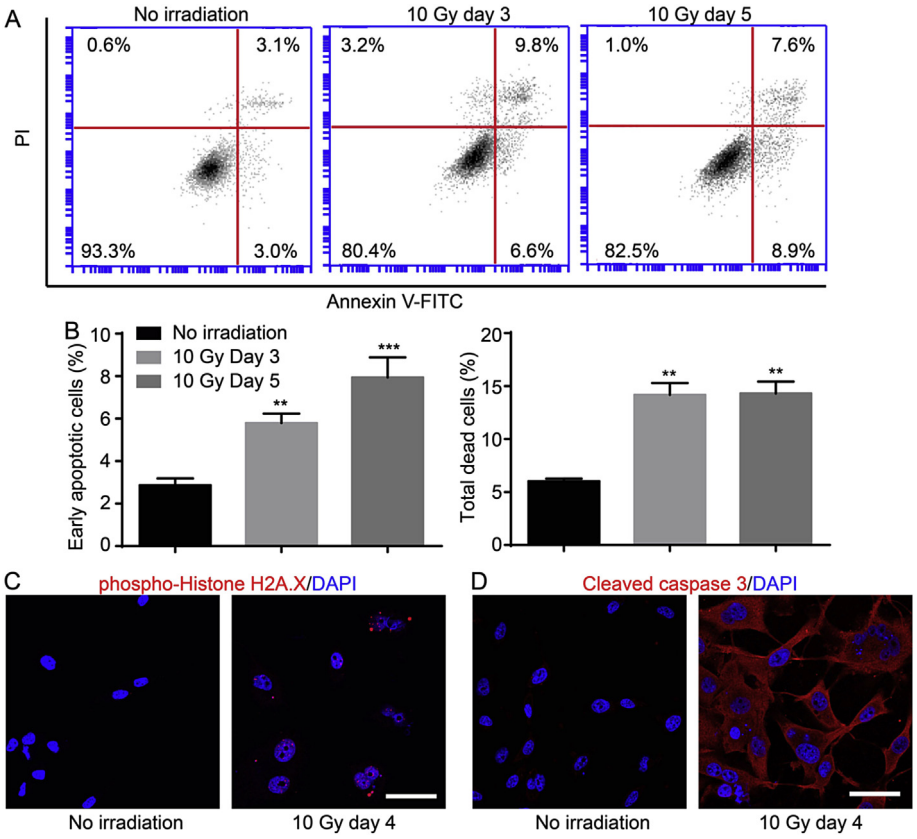

Fig. 2. X-irradiation leads to DNA damage and caspase 3 activation in dying glioma cells. **A**. Representative flow cytometry plots displaying U87 cell death in response to 10 Gy irradiation. **B**. Quantification analysis showing percentages of early apoptosis and total cell death of U87 cells following 10 Gy irradiation. $^{**}p < 0.01$, $^{***}p < 0.001$, compared with no irradiation, one-way ANOVA, LSD, n = 3. **C**. Confocal immunofluorescence analysis exhibiting the formation of H2A.X foci in 10 Gy-irradiated U87 cells. Scale bar: 50 μm. **D**. Confocal immunofluorescence analysis showing caspase 3 activation in 10 Gy-irradiated U87 cells. Scale bar: 50 μm.

period, proliferation of HUVEC-Fluc or HMEC-1-Fluc was detected by bioluminescence imaging. To test the validity of measuring endothelial cell proliferation by luciferase activity, we showed that bioluminescence values were tightly correlated with cell number in both HUVEC-Fluc and HMEC-1-Fluc (Fig. 1A, C). Subsequent results displayed that irradiated U87 cells prompted HUVEC-Fluc proliferation in a dose-dependent manner (Fig. 1B) and 10 Gy-irradiated U87 cells also exerted strong proliferation-stimulating effect on HMEC-1-Fluc (Fig. 1D). In addition, 10 Gy-irradiated U87 cells strongly stimulated HUVEC-Fluc proliferation when HUVEC-Fluc were seeded in hanging cell culture inserts, therefore disclosing that irradiated glioma cells secreted some soluble substances, which operate in this proliferation-stimulating process (Fig. 1E). Besides strong proliferation-prompting effect of irradiated glioma cells on endothelial cells, we also examined whether irradiated glioma cells could induce endothelial migration. Compared with conditioned media (CM) collected from non-irradiated U87 cells, CM from 10 Gy-irradiated U87 cells notably evoked HUVEC migration (Fig. 1F). Taken together, these data demonstrated that irradiated glioma cells vigorously activated endothelial cells by promoting their proliferation and migration, in which soluble factors secreted from irradiated glioma cells participated.

X-irradiation induces DNA damage and caspase 3 activation in dying glioma cells

It has been generally held that X-irradiation is able to induce tumor cell death. To determine the death manner of U87 cells in response to X-irradiation, we employed flow cytometry analysis through FITC Annexin V and propidium iodide (PI) double staining. We observed that following 10 Gy irradiation the percentage of U87 cells in early apoptosis (FITC Annexin V positive and PI negative) notably rose in a day-dependent manner (Fig. 2A and B). In addition, the percentage of total cell death (FITC Annexin V positive) was significantly higher on day 3 and 5 after 10 Gy irradiation than before irradiation (Fig. 2A and B). Subsequently, immunofluorescence analysis showed the formation of phosphorylated histone H2A.X foci (Fig. 2C) and expression of cleaved caspase 3 (Fig. 2D) in U87 cells four days after 10 Gy irradiation, at molecular level indicating DNA damage and apoptosis activation in response to irradiation. In sum, these data verified that 10 Gy irradiation did induce glioma cell death, accompanied with DNA damage and caspase 3 activation.

Caspase 3 inhibition in dying glioma cells reduces their proangiogenic effects in vitro and in vivo

Increasing studies have uncovered the growth-promoting role of caspase 3 in multiple scenarios, such as wound healing and tissue regeneration [21], tumor repopulation [22] and osteoclastogenesis [23]. In addition, our previous study has shown that caspase 3 in dying colorectal cancer cells mediates post-irradiation angiogenesis [28]. We therefore hypothesized that caspase 3 of dying glioma cells may play a vital role in the proangiogenic process after irradiation. To inhibit caspase 3 activity, we firstly transduced a dominant-negative caspase 3 gene (C163A) into U87 cells, named as U87 CASP3DN. Western blot analysis validated the expression of dominant-negative version of caspase 3 in U87 CASP3DN cells by

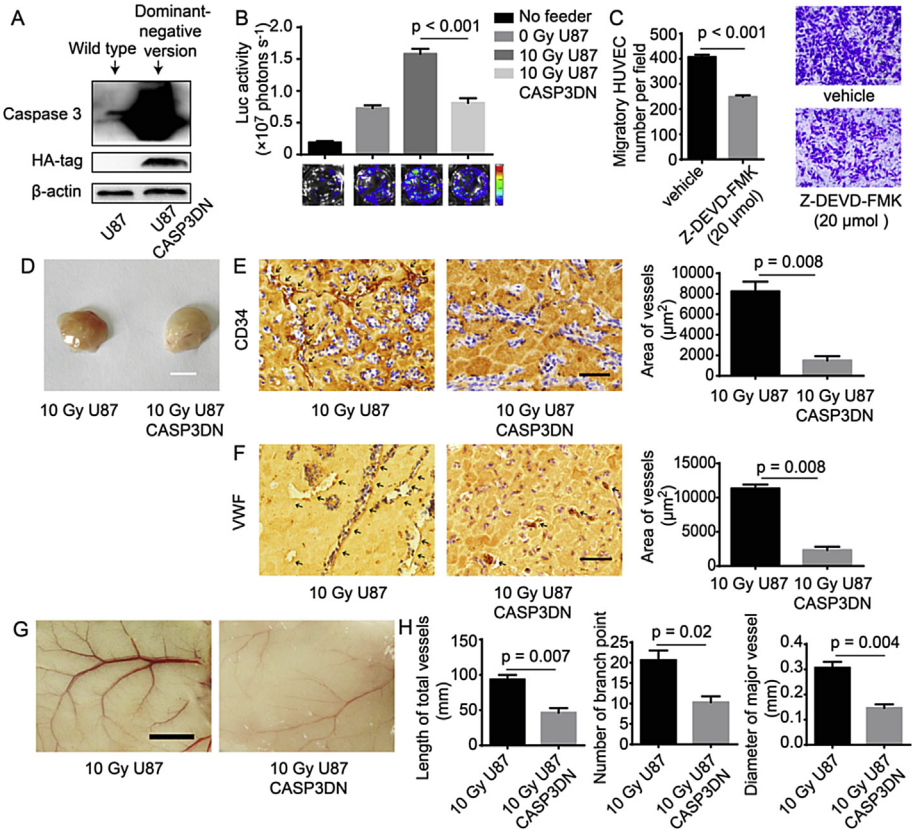

Fig. 3. Caspase 3 inhibition weakens proangiogenic response after irradiation *in vitro* and *in vivo*. **A**. Western blot analysis confirmed the expression of dominant-negative caspase 3 by detecting tandemly-fused HA-tag and overexpressed dominant-negative caspase 3. **B**. Proliferation-promoting effect of dying U87 CASP3DN cells on HUVEC-Fluc was significantly impaired, compared with equally treated parental U87 cells ($p < 0.001$, one-way ANOVA, LSD, $n = 4$). **C**. Left panel, quantification analysis depicting HUVEC migration towards CM collected from 10 Gy-irradiated U87 cells treated with vehicle or Z-DEVD-FMK ($p < 0.001$, Student's *t*-test, $n = 5$). Right panel, representative images of HUVEC migration towards indicated CM. Scale bar: 250 μm. **D**. Representative picture showing matrigel plugs mixed with 10 Gy-irradiated U87 or U87 CASP3DN cells ($n = 3$). Scale bar: 5 mm. **E** and **F**. Left panel, immunohistochemical staining for CD34 or VWF of plug sections. Scale bar: 50 μm. Right panel, quantification analysis of area of blood vessels ($p = 0.008$, Mann−Whitney *U* test, $n = 5$). **G**. Representative images of skin vasculature adjoining indicated plugs. Scale bar: 5 mm. **H**. Quantification analysis of dermal vasculature adjoining plugs from length of vessels, number of branch point and diameter of major vessel (Student's *t*-test, $n = 3$).

detecting tandemly-inserted hemagglutinin (HA)-tag and overexpressed dominant-negative caspase 3 (Fig. 3A). Notably, by utilizing the foregoing *in vitro* coculture model, we noticed that 10 Gy-irradiated U87 CASP3DN cells displayed significantly weakened proliferation-prompting effect on HUVEC-Fluc, compared with equally irradiated U87 cells (Fig. 3B). Additionally, we collected CM from 10 Gy-irradiated U87 cells treated with vehicle or caspase 3 inhibitor, Z-DEVD-FMK, and tested their pro-migratory ability. Results showed that HUVEC migration toward CM from irradiated U87 treated with Z-DEVD-FMK was significantly decreased compared with control (Fig. 3C). Having validated that caspase 3 in dying glioma cells mediates proangiogenic response *in vitro*, we next determined whether caspase 3 participates in the proangiogenic process *in vivo* by conducting matrigel plug assay. We found that blood vessel formation in matrigel mixed with 10 Gy-irradiated U87 CASP3DN cells was markedly reduced, compared with control (Fig. 3D). Immunohistochemical staining of matrigel plug sections for angiogenesis markers, CD34 and VWF, further substantiated our macroscopic observation (Fig. 3E and F). Furthermore, skin vascularization adjoining plugs containing 10 Gy-irradiated U87 CASP3DN cells was highly less than control from three aspects: length of vessels, number of branch point and diameter of major vessels (Fig. 3G and H). Overall, evidence *in vitro* and *in vivo* indicated that caspase 3 in dying glioma cells mediated proangiogenic response after irradiation.

Proteolytic inactivity of caspase 3 in glioma cells represses tumorigenicity

We explored the role of caspase 3 in tumorigenicity by performing tumor xenograft assay. Considering that glioma cell death occurs in the absence of irradiation (Fig. 2A and B), we supposed that caspase 3 inactivity may reduce tumorigenicity because those naturally dying glioma cells with caspase 3 inactivity have impaired ability to elicit tumor angiogenesis. Intriguingly, in line with our assumption, U87 CASP3DN cells displayed sharply reduced tumorigenicity, compared with parental U87 cells (Fig. 4A and B).

In silico analysis of correlation between CASP3 and angiogenesis markers

Having indicated that inhibition of caspase 3 activity in dying glioma cells reduces their proangiogenic effects, we subsequently explored whether caspase 3, at expression level, is associated with angiogenesis markers in human specimens. We employed 169 RNA-seq data from 161 GBM patients in TCGA. Spearman correlation analysis revealed statistically significant correlation between CASP3 and PECAM1 or KDR (Fig. 4C, E), while the correlation between CASP3 and FLT1 is not statistically significant (Fig. 4D). To further examine these correlations, we also utilized the microarray data of 220 glioma patients from CGGA. Spearman

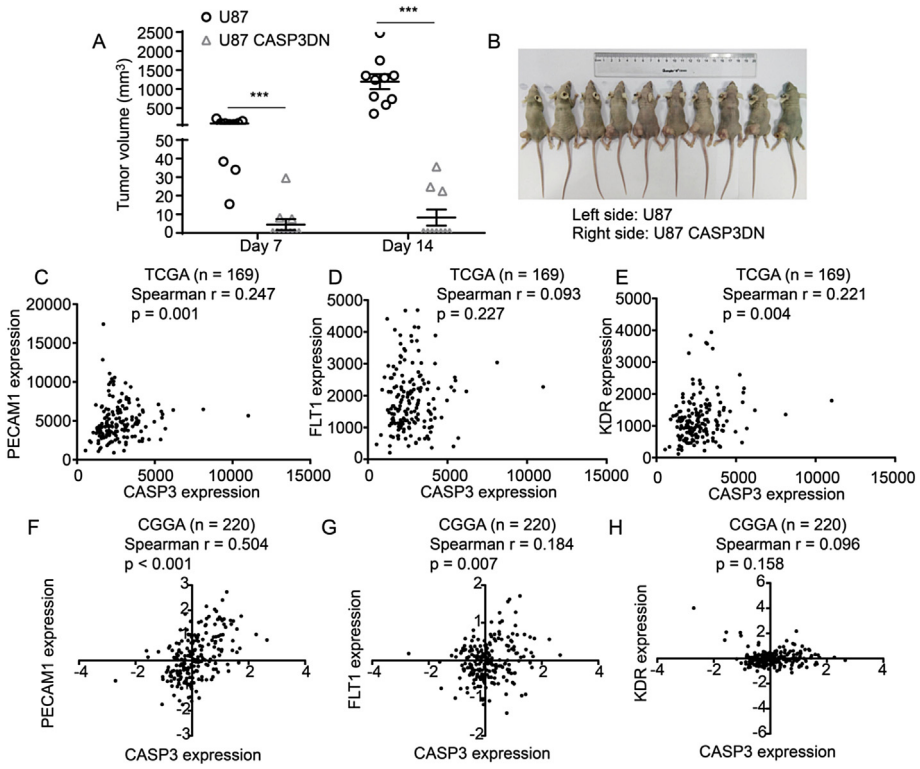

Fig. 4. Proteolytic inactivation of caspase 3 reduces tumorigenicity and *in silico* analyses of correlations between CASP3 and angiogenesis markers. **A**. Plot showing tumorigenicity of U87 and U87 CASP3DN cells in tumor xenograft assay (***$p < 0.001$, Mann–Whitney *U* test, $n = 10$). **B**. Photograph showing nude mice bearing U87 and U87 CASP3DN xenograft. **C**–**E**. Spearman correlation analysis between CASP3 and PECAM1, FLT1 or KDR in 169 GBM specimens from 161 GBM cases using RNA-seq data from TCGA. **F**–**H**. Spearman correlation analysis between CASP3 and PECAM1, FLT1 or KDR in 220 glioma patients using microarray data from CGGA.

correlation analysis revealed statistically significant correlation between CASP3 and PECAM1 or FLT1 (Fig. 4F and G), while the correlation between CASP3 and KDR is not statistically significant (Fig. 4H).

NF-κB/COX-2/PGE$_2$: one downstream axis of caspase 3 in post-irradiation angiogenesis

The foregoing results manifested that the proangiogenic response of dying glioma cells was mediated by soluble factors, so what downstream factors of caspase 3 operate in this process? Our previous studies show that PGE_2 act as a downstream factor of caspase 3, mediating tissue regeneration [21] and tumor repopulation [22]. Thereby, we hypothesized that caspase 3 may control PGE_2 production through regulating COX-2 expression, which is the key enzyme in PGE_2 synthesis process. Interestingly, western blot analysis showed that the induction of COX-2 and NF-κB (phosph-p65), the well-known transcription factor of COX-2, in response to irradiation was markedly suppressed in U87 CASP3DN cells, compared with parental U87 cells (Fig. 5A and B). Western blot analysis also showed that the expression of cleaved caspase 3 occurred since day 1 after 10 Gy irradiation and was earlier than induction of phosph-p65 and COX-2, which further suggested that NF-κB/COX-2 is a downstream axis of caspase 3 (Fig. 5C). Furthermore, ELISA corroborated that PGE_2 concentration of supernatants from irradiated U87 CASP3DN cells is much lower than control (Fig. 5D). To substantiate that COX-2/PGE_2 axis mediates proangiogenic response of dying glioma cells, we explored whether post-irradiation angiogenesis was weakened when COX-2 was inhibited. Result showed that NS-398, a COX-2 inhibitor, notably reduced proliferation-promoting effect of dying glioma cells on HUVEC-Fluc (Fig. 5E). Moreover, HUVEC migration toward CM from irradiated U87 treated with NS-398 was significantly diminished compared with control (Fig. 5F).

VEGF-A: another downstream proangiogenic factor of caspase 3

Previous studies have indicated that caspase 3 activity inhibition disrupts VEGF release from dying cells [23,29]. We therefore determine whether VEGF acts as a downstream proangiogenic factor of caspase 3 and mediates the proangiogenic response. ELISA showed that Z-DEVD-FMK significantly suppressed VEGF-A release from 10 Gy-irradiated U87 cells, suggesting that VEGF-A is regulated by caspase 3 activity in dying glioma cells (Fig. 6A). In addition, eIF4E was considered to play a rate-limiting role in driving translation of VEGF [30]. Intriguingly, western blot analysis manifested that the phosphorylation of eIF4E in response to irradiation was inhibited when caspase 3 was inactivated (Fig. 6B), implying that caspase 3 activity regulates VEGF expression possibly via phosphorylation of eIF4E. To further substantiate that VEGF mediates the proangiogenic effects of dying glioma cells, we studied whether proangiogenic response was extenuated when VEGF was pharmacologically inhibited. We observed that Ki8751, a VEGF receptor 2 inhibitor, notably disrupted the proliferation-promoting effect of dying U87 cells on HUVEC-Fluc, while the concentration of Ki8751 used did not influence HUVEC-Fluc proliferation alone (Fig. 6C). Furthermore, 1 μmol Ki8751 also significantly inhibited the migration of HUVEC towards CM from 10 Gy-irradiated U87 cells (Fig. 6D). Finally, a diagram schematically summarized the caspase 3-initiating proangiogenic process (Fig. 6E).

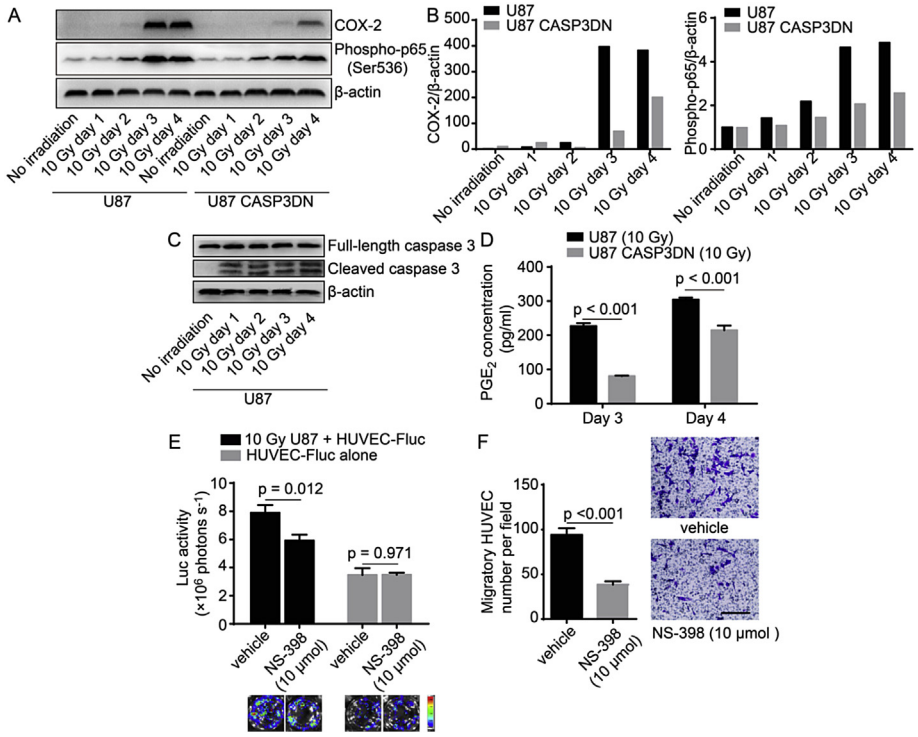

Fig. 5. NF-κB/COX-2/PGE_2 axis serves as one downstream effector of caspase 3, mediating post-irradiation angiogenesis. **A**. Western blot analysis indicating that the induction of COX-2 and phosph-p65 in response to irradiation was inhibited when caspase 3 was inactivated. **B**. Quantification analysis showing that the expression of COX-2 and phosph-p65 was less induced by irradiation in U87 CASP3DN cells than in parental U87 cells. **C**. Western blot analysis showed that the expression of cleaved caspase 3 in U87 cells after 10 Gy irradiation occurred since day 1. **D**. ELISA revealing that PGE_2 concentration of CM was highly decreased when caspase 3 was inactivated (one-way ANOVA, LSD, n = 3). **E**. NS-398, a COX-2 inhibitor, extenuated the proliferation-stimulating effect of dying U87 cells on HUVEC-Fluc (one-way ANOVA, LSD, n = 3). **F**. Left panel, quantification analysis displaying HUVEC migration towards CM collected from 10 Gy-irradiated U87 cells treated with vehicle or NS-398 ($p < 0.001$, Student's *t*-test, n = 5). Right panel, representative images of HUVEC migration towards indicated CM. Scale bar: 250 μm.

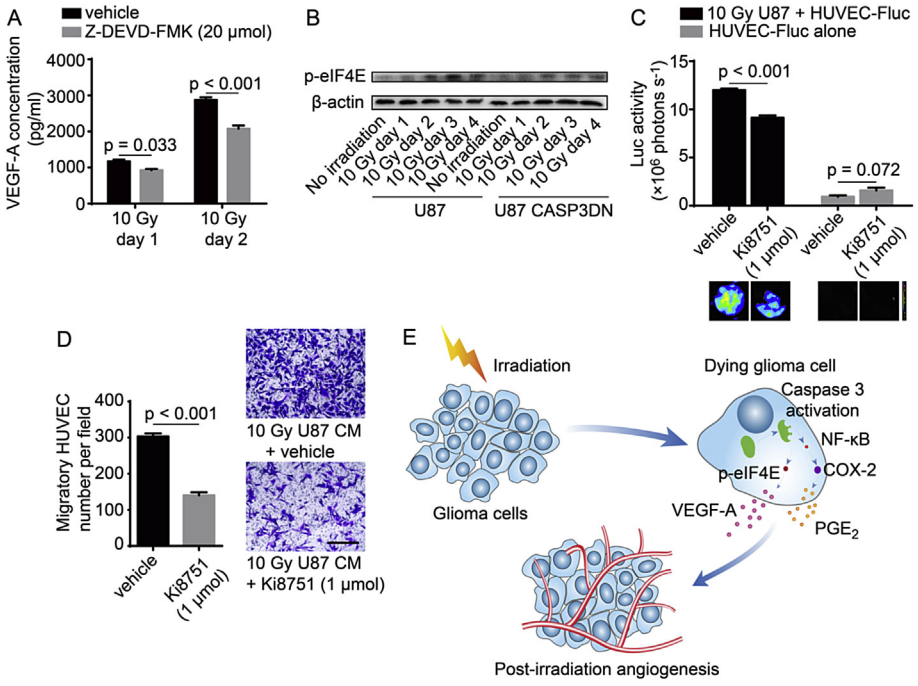

Fig. 6. VEGF-A was another downstream proangiogenic factor of caspase 3. **A**. ELISA showing that VEGF-A concentrations of CM collected from 10 Gy-irradiated U87 cells treated with caspase 3 inhibitor, Z-DEVD-FMK, was much lower than controls (one-way ANOVA, LSD, n = 3). **B**. p-eIF4E induction in response to irradiation was inhibited when caspase 3 was inactivated. **C**. Ki8751, a VEGFR2 inhibitor, significantly mitigated the proliferation-stimulating effect of dying U87 cells on HUVEC-Fluc (one-way ANOVA, LSD, n = 3). **D**. Left panel, quantification analysis showing that Ki8751 decreased HUVEC migration towards CM from irradiated U87 cells ($p < 0.001$, Student's *t*-test, n = 5). Right panel, representative images of HUVEC migration with or without administration of Ki8751 towards CM from irradiated U87 cells. Scale bar: 250 μm. **E**. A schematic representation of mechanisms underlying post-irradiation angiogenesis elicited by dying glioma cells.

Discussion

Killing tumor cells has long been a dogmatic strategy in cytotoxic cancer treatments like radiotherapy. However, our results unexpectedly demonstrated that irradiation-induced dying glioma cells unfavorably establish a proangiogenic microenvironment. This post-irradiation angiogenesis inflicted by dying cells would contribute to radioresistance or tumor recurrence, because it has been indicated that endothelial radiosensitivity crucially regulates tumor response to radiotherapy [31]. While inducing caspase 3 activation has been extensively used for radiosensitization in cancer therapeutics, our data counterintuitively showed that inhibition of caspase 3 activation in dying glioma cells remarkably reduced their proangiogenic effects after irradiation. Interestingly, proteolytic inactivity of caspase 3 unexpectedly suppressed tumorigenicity. Moreover, *in silico* analysis revealed some positive correlations between CASP3 and angiogenesis markers. Finally, we identified two downstream targets of caspase 3, NF-κB/COX-2/PGE_2 and VEGF-A, which involved in post-irradiation angiogenesis.

Though it seems paradoxical to connect caspase 3, a key executioner in apoptosis, with proangiogenic effects, several studies have already suggested similar findings. One study exhibited that caspase 3 deletion markedly abrogated the proangiogenic ability of irradiated mouse embryonic fibroblasts [21]. Another study demonstrated that inhibition of caspase 3 activity diminished the proangiogenic response of lipid-injured hepatocytes [29]. What is more important, besides proangiogenic effects, emerging studies have clarified growth-prompting role of caspase 3 in multiple physiopathological processes, such as fibrosis [20], wounding healing and tissue regeneration [21], tumor repopulation [22], osteoclastogenesis [23] and oncogenesis [24]. Accordingly, these newly discovered roles of caspase 3 lead us to assume that caspase 3 may play a double-edged role influencing both cell death and survival.

In this study, using GBM data from TCGA revealed significant correlation between CASP3 and PECAM1 or KDR (Fig. 4C, E). Additional analysis using microarray data from CGGA uncovered significant correlation between CASP3 and PECAM1 or FLT1 (Fig. 4F and G). Not surprisingly, tumor angiogenesis has already been associated with metastasis [32], recurrence [33] and poor prognosis [34,35]. Therefore, we raise the question that whether higher levels of CASP3 expression represent poor prognosis. Intriguingly, the Kaplan–Meier analysis of survival in 249 breast cancer patients revealed that the group of patients with higher CASP3 expression bore worse survival probability [22]. However, using 161 GBM data from TCGA, we found that though higher CASP3 expression in GBMs seemingly correlates with lower survival time, the difference is not statistically significant ($p = 0.25489$, data not shown). It is possible that the correlation between CASP3 expression and survival rate varies among different cancers. Also, we should interpret this result with caution due to limited sample size.

We identified COX-2/PGE_2 axis as downstream signalings of caspase 3, mediating proangiogenic response. Similarly, a recent study [36] showed that DNLD, a specific caspase 3 inhibitor, significantly reduced chemotherapy induced COX-2 upregulation and PGE_2 release, corroborating that COX-2/PGE_2 axis acted as downstream effectors of caspase 3. In addition, our data also showed that inhibition of caspase 3 activity significantly reduced irradiation-induced VEGF-A secretion. Consistent with this result, another study displayed that pharmacologically inhibiting caspase 3 activity blocks fatigue-induced VEGF upregulation in osteocytes [23].

One potential application of this study implicates that radiotherapy in combination with caspase 3 inhibitors may be more effective in tumor control due to restricted post-irradiation angiogenesis. Indeed, evidence showed that M867, a selective caspase 3 inhibitor, radiosensitizes non-small cell lung cancer xenograft *in vivo* [37]. In addition, ionizing irradiation combined with administration of M867 yielded a marked tumor growth delay compared with irradiation alone, with dramatic reduction in tumor vasculature [38]. These pioneering studies lead us to develop novel therapeutic strategies that combine radiotherapy and caspase 3 inhibitors.

In sum, we hope this caspase 3-centered proangiogenic mechanism would arouse more interest in prospective studies and provide more effective therapeutic targets for cancer radiotherapy.

Acknowledgements

We are thankful for the funding of National Natural Science Foundation of China (81120108017, 81572951) (Qian Huang), (81172030) (Ling Tian), (81502648) (Jin Cheng), (81572788) (Xinjian Liu) and grants from National Institutes of Health, USA (ES024015, CA155270) (Chuan-Yuan Li).

Conflicts of interest

The authors state no conflicts of interest.

Appendix A. Supplementary data

Supplementary data related to this article can be found at http://dx.doi.org/10.1016/j.canlet.2016.10.042.

References

[1] J.A. Schwartzbaum, J.L. Fisher, K.D. Aldape, M. Wrensch, Epidemiology and molecular pathology of glioma, Nature clinical practice, Neurology 2 (2006) 494–503.
[2] H. Sontheimer, Brain cancer: tumour cells on neighbourhood watch, Nature 528 (2015) 49–50.
[3] E.K. Lehrman, B. Stevens, Shedding light on glioma growth, Cell 161 (2015) 704–706.
[4] M.S. Bovenberg, M.H. Degeling, B.A. Tannous, Advances in stem cell therapy against gliomas, Trends Mol. Med. 19 (2013) 281–291.
[5] T. VandenDriessche, M.K. Chuah, Glioblastoma: bridging the gap with gene therapy, Lancet Oncol. 14 (2013) 789–790.
[6] R.L. Sabado, N. Bhardwaj, Cancer immunotherapy: dendritic-cell vaccines on the move, Nature 519 (2015) 300–301.
[7] D. Sehedic, A. Cikankowitz, F. Hindre, F. Davodeau, E. Garcion, Nanomedicine to overcome radioresistance in glioblastoma stem-like cells and surviving clones, Trends Pharmacol. Sci. 36 (2015) 236–252.
[8] J. Chen, Y. Li, T.S. Yu, R.M. McKay, D.K. Burns, S.G. Kernie, et al., A restricted cell population propagates glioblastoma growth after chemotherapy, Nature 488 (2012) 522–526.
[9] B.E. Johnson, T. Mazor, C. Hong, M. Barnes, K. Aihara, C.Y. McLean, et al., Mutational analysis reveals the origin and therapy-driven evolution of recurrent glioma, Science (New York, N.Y.) 343 (2014) 189–193.
[10] D.A. Nathanson, B. Gini, J. Mottahedeh, K. Visnyei, T. Koga, G. Gomez, et al., Targeted therapy resistance mediated by dynamic regulation of extrachromosomal mutant EGFR DNA, Science (New York, N.Y.) 343 (2014) 72–76.
[11] K. Tanaka, T. Sasayama, Y. Irino, K. Takata, H. Nagashima, N. Satoh, et al., Compensatory glutamine metabolism promotes glioblastoma resistance to mTOR inhibitor treatment, J. Clin. Investigation 125 (2015) 1591–1602.
[12] M. Osswald, E. Jung, F. Sahm, G. Solecki, V. Venkataramani, J. Blaes, et al., Brain tumour cells interconnect to a functional and resistant network, Nature 528 (2015) 93–98.
[13] I.J. Barani, D.A. Larson, Radiation therapy of glioblastoma, Cancer Treat. Res. 163 (2015) 49–73.
[14] J.P. Kirkpatrick, J.H. Sampson, Recurrent malignant gliomas, Semin. Radiat. Oncol. 24 (2014) 289–298.
[15] R.K. Jain, E. di Tomaso, D.G. Duda, J.S. Loeffler, A.G. Sorensen, T.T. Batchelor, Angiogenesis in brain tumours, Nature reviews, Neuroscience 8 (2007) 610–622.
[16] M. Kioi, H. Vogel, G. Schultz, R.M. Hoffman, G.R. Harsh, J.M. Brown, Inhibition of vasculogenesis, but not angiogenesis, prevents the recurrence of glioblastoma after irradiation in mice, J. Clin. Invest. 120 (2010) 694–705.
[17] E. Tabouret, A. Tchoghandjian, E. Denicolai, C. Delfino, P. Metellus, T. Graillon, et al., Recurrence of glioblastoma after radio-chemotherapy is associated with

an angiogenic switch to the CXCL12-CXCR4 pathway, Oncotarget 6 (2015) 11664–11675.
[18] S. Asuthkar, K.K. Velpula, A.K. Nalla, V.R. Gogineni, C.S. Gondi, J.S. Rao, Irradiation-induced angiogenesis is associated with an MMP-9-miR-494-syndecan-1 regulatory loop in medulloblastoma cells, Oncogene 33 (2014) 1922–1933.
[19] Y. Liu, L. Zhang, Y. Liu, C. Sun, H. Zhang, G. Miao, et al., DNA-PKcs deficiency inhibits glioblastoma cell-derived angiogenesis after ionizing radiation, J. Cell. Physiol. 230 (2015) 1094–1103.
[20] P. Laplante, I. Sirois, M.A. Raymond, V. Kokta, A. Beliveau, A. Prat, et al., Caspase-3-mediated secretion of connective tissue growth factor by apoptotic endothelial cells promotes fibrosis, Cell Death Differ. 17 (2010) 291–303.
[21] F. Li, Q. Huang, J. Chen, Y. Peng, D.R. Roop, J.S. Bedford, C.Y. Li, Apoptotic cells activate the “phoenix rising” pathway to promote wound healing and tissue regeneration, Sci. Signal. 3 (2010) ra13.
[22] Q. Huang, F. Li, X. Liu, W. Li, W. Shi, F.F. Liu, et al., Caspase 3-mediated stimulation of tumor cell repopulation during cancer radiotherapy, Nat. Med. 17 (2011) 860–866.
[23] O.D. Kennedy, D.M. Laudier, R.J. Majeska, H.B. Sun, M.B. Schaffler, Osteocyte apoptosis is required for production of osteoclastogenic signals following bone fatigue in vivo, Bone 64 (2014) 132–137.
[24] X. Liu, Y. He, F. Li, Q. Huang, T.A. Kato, R.P. Hall, et al., Caspase-3 promotes genetic instability and carcinogenesis, Mol. Cell 58 (2015) 284–296.
[25] J. Cheng, L. Tian, J. Ma, Y. Gong, Z. Zhang, Z. Chen, et al., Dying tumor cells stimulate proliferation of living tumor cells via caspase-dependent protein kinase Cdelta activation in pancreatic ductal adenocarcinoma, Mol. Oncol. 9 (2015) 105–114.
[26] Z. Zhang, M. Wang, L. Zhou, X. Feng, J. Cheng, Y. Yu, et al., Increased HMGB1 and cleaved caspase-3 stimulate the proliferation of tumor cells and are correlated with the poor prognosis in colorectal cancer, J. Exp. Clin. Cancer Res. 34 (2015) 51.
[27] S. Anders, D.J. McCarthy, Y. Chen, M. Okoniewski, G.K. Smyth, W. Huber, et al., Count-based differential expression analysis of RNA sequencing data using R and Bioconductor, Nat. Protoc. 8 (2013) 1765–1786.
[28] X. Feng, L. Tian, Z. Zhang, Y. Yu, J. Cheng, Y. Gong, et al., Caspase 3 in dying tumor cells mediates post-irradiation angiogenesis, Oncotarget 6 (2015) 32353–32367.
[29] D. Povero, A. Eguchi, I.R. Niesman, N. Andronikou, X. de Mollerat du Jeu, A. Mulya, et al., Lipid-induced toxicity stimulates hepatocytes to release angiogenic microparticles that require Vanin-1 for uptake by endothelial cells, Sci. Signal. 6 (2013) ra88.
[30] C. Lu, L. Makala, D. Wu, Y. Cai, Targeting translation: eIF4E as an emerging anticancer drug target, Expert Rev. Mol. Med. 18 (2016) e2.
[31] M. Garcia-Barros, F. Paris, C. Cordon-Cardo, D. Lyden, S. Rafii, A. Haimovitz-Friedman, et al., Tumor response to radiotherapy regulated by endothelial cell apoptosis, Science (New York, N.Y.) 300 (2003) 1155–1159.
[32] B.R. Zetter, Angiogenesis and tumor metastasis, Annu. Rev. Med. 49 (1998) 407–424.
[33] K. Maeda, Y.S. Chung, S. Takatsuka, Y. Ogawa, T. Sawada, Y. Yamashita, et al., Tumor angiogenesis as a predictor of recurrence in gastric carcinoma, J. Clin. Oncol. 13 (1995) 477–481.
[34] G. Gasparini, A.L. Harris, Clinical importance of the determination of tumor angiogenesis in breast carcinoma: much more than a new prognostic tool, J. Clin. Oncol. 13 (1995) 765–782.
[35] D. Meitar, S.E. Crawford, A.W. Rademaker, S.L. Cohn, Tumor angiogenesis correlates with metastatic disease, N-myc amplification, and poor outcome in human neuroblastoma, J. Clin. Oncol. 14 (1996) 405–414.
[36] L. Flanagan, M. Meyer, J. Fay, S. Curry, O. Bacon, H. Duessmann, et al., Low levels of Caspase-3 predict favourable response to 5FU-based chemotherapy in advanced colorectal cancer: caspase-3 inhibition as a therapeutic approach, Cell Death Dis. 7 (2016) e2087.
[37] B. Li, J.M. Blanc, Y. Sun, L. Yang, N.G. Zaorsky, N.J. Giacalone, et al., Assessment of M867, a selective caspase-3 inhibitor, in an orthotopic mouse model for non-small cell lung carcinoma, Am. J. Cancer Res. 4 (2014) 161–171.
[38] K.W. Kim, L. Moretti, B. Lu, M867, a novel selective inhibitor of caspase-3 enhances cell death and extends tumor growth delay in irradiated lung cancer models, PLoS One 3 (2008) e2275.